doi:10.1006/jmbi.2000.3601 available online at http://www.idealibrary.com on IDEAL® *J. Mol. Biol.* (2000) **297**, 615–626

JMB

Visualization of the Maturation Transition in Bacteriophage P22 by Electron Cryomicroscopy

Zhixian Zhang[1], Barrie Greene[2], Pamela A. Thuman-Commike[1] Joanita Jakana[1], Peter E. Prevelige Jr[3], Jonathan King[2] and Wah Chiu[1]*

[1]*Verna and Marrs McLean Department of Biochemistry and Molecular Biology, Baylor College of Medicine, One Baylor Plaza, Houston TX 77030, USA*

[2]*Department of Biology Massachusetts Institute of Technology, Cambridge MA 02139, USA*

[3]*Department of Microbiology University of Alabama at Birmingham, Birmingham AL 35294, USA*

**Corresponding author*

Large-scale conformational transitions are involved in the life-cycle of many types of virus. The dsDNA phages, herpesviruses, and adenoviruses must undergo a maturation transition in the course of DNA packaging to convert a scaffolding-containing precursor capsid to the DNA-containing mature virion. This conformational transition converts the procapsid, which is smaller, rounder, and displays a distinctive skewing of the hexameric capsomeres, to the mature virion, which is larger and more angular, with regular hexons. We have used electron cryomicroscopy and image reconstruction to obtain 15 Å structures of both bacteriophage P22 procapsids and mature phage. The maturation transition from the procapsid to the phage results in several changes in both the conformations of the individual coat protein subunits and the interactions between neighboring subunits. The most extensive conformational transformation among these is the outward movement of the trimer clusters present at all strict and local 3-fold axes on the procapsid inner surface. As the trimer tips are the sites of scaffolding binding, this helps to explain the role of scaffolding protein in regulating assembly and maturation. We also observe DNA within the capsid packed in a manner consistent with the spool model. These structures allow us to suggest how the binding interactions of scaffolding and DNA with the coat shell may act to control the packaging of the DNA into the expanding procapsids.

Keywords: bacteriophage P22; DNA arrangement; DNA packaging; electron cryomicroscopy; maturation transition

Introduction

A common theme in virus assembly is large-scale conformational transitions of viral capsids associated with specific events in the viral life-cycle. The binding of polioviruses and rhinoviruses to their cell receptors induces conformational changes, resulting in uncoating and release of viral RNA into the cell (Rueckert, 1996). This transition is similar to the expansion of plant viruses upon depletion of divalent cations at alkaline pH (Incardona & Kaesberg, 1964; Robinson & Harrison, 1982). For plant viruses, the expanded form is thought to represent an intermediate in the disassembly and infection process. In the case of the isometric dsDNA bacteriophages, herpesviruses, and adenoviruses, the initial product of assembly is not the DNA-containing virion, but a precursor capsid, or procapsid (Casjens & Hendrix, 1988; D'Halluin *et al*., 1978; Rixon, 1993). These procapsids lack DNA, but contain hundreds of protein molecules not found in the mature virion, termed scaffolding proteins (King & Casjens, 1974). A critical step in assembly of these viruses, therefore, is capsid maturation, the transition of the assembled coat protein shell from the procapsid state to the mature virion state.

The differences between the two capsid structures are not limited to the procapsid containing scaffolding protein and the DNA of the mature virion. Electron cryomicroscopy and image reconstruction have revealed characteristic differences in the conformation and arrangement of the coat

Present addresses: B. Green, Incyte Pharmaceuticals, 3174 Porter Dr., Palo Alto, CA 94304, USA; P. A. Thuman-Commike, QED Labs, 1190 S. Boscom Ave., Suite 208, San Jose, CA 95128, USA.

E-mail address of the corresponding author: wah@bcm.tmc.edu

0022-2836/00/030615–12 $35.00/0

subunits between procapsids and mature virions from bacteriophages P22, λ, and HK97 (Conway *et al*., 1995; Dokland & Murialdo, 1993; Prasad *et al*., 1993) as well as herpesvirus (Trus *et al*., 1996). With the exception of the herpesvirus procapsid, which is not smaller than the mature virion (Trus *et al*., 1996), procapsids are smaller, rounder, and display a distinctive skewing of the hexameric capsomeres. In contrast, the mature virion is larger and more angular, with regular hexons possessing 6-fold symmetry. In many cases, these pronounced structural transitions occur in the absence of any proteolytic cleavages or covalent modifications of the viral coat proteins (Casjens & Hendrix, 1988).

During maturation, several processes occur: the scaffolding molecules are released from the procapsid, in a process that may or may not involve proteolytic cleavage of the scaffolding subunits (DiIanni *et al*., 1993; King & Casjens, 1974; Nelson *et al*., 1976; Onorato & Showe, 1975; Ray & Murialdo, 1975); DNA is packaged into the capsid in a process that requires phage-encoded packaging proteins and ATP (Black, 1989); and the coat lattice undergoes conformational transitions leading to the mature structure. The order and causality of these events is still uncertain.

The maturation transition has been particularly well studied for bacteriophage P22, a $T = 7$ isometric phage of *Salmonella typhimurium* (Figure 1). Assembly of P22 procapsid requires approximately 300 scaffolding subunits in addition to the 420 coat subunits (Casjens & King, 1974). DNA is packaged through a specialized vertex at one of the 5-fold symmetry axes that contains a dodecameric portal protein complex (Bazinet & King, 1985). During phage maturation, all the scaffolding subunits are released intact, and are recycled into newly assembling procapsids (King & Casjens, 1974). Structures of both procapsid and phage at 30 Å resolution from electron cryomicroscopy and image reconstruction suggested channels at the centers of the skewed hexons that were closed in the phage, and may be the sites for scaffolding exit (Prasad *et al*., 1993). Raman spectroscopy of procapsid and phage structures demonstrated that the coat protein is significantly more protected from solvent exposure in the phage than the procapsid (Tuma *et al*., 1998).

Expansion of P22 procapsid to the mature form can be induced *in vitro* by heating (Galisteo & King, 1993). Differential scanning calorimetry of procapsids showed that the maturation transition is exothermic, demonstrating that the phage structure is a lower energy state than the procapsid (Galisteo & King, 1993). The mature capsid of phage T4 is also more stable than the T4 procapsid and occupies a lower energy state (Ross *et al*., 1985; Steven *et al*., 1992). The maturation transition is not reversible for any of the dsDNA phages, providing directionality to the assembly pathway. Thus, the procapsid may be considered a metastable intermediate on the pathway to the mature virion.

An intriguing question is why the assembly pathway for these viruses must proceed through a procapsid intermediate. It may be that the conformational requirements for assembly and scaffolding binding are incompatible with the structure of the mature virion, which is designed for optimal stability and protection of the encapsidated DNA. The structure of the procapsid may also be optimized for its function as a DNA packaging machine, while the virion must be designed to release DNA during infection (King & Chiu, 1997).

To address these issues, we used electron cryomicroscopy and image reconstruction to obtain 15 Å structures of both P22 procapsid and mature phage. At this resolution, domain motions involved in the maturation transition can be observed, helping to elucidate the structural mechanism of expansion. These structures, combined with other recent structural and biochemical studies of P22, allow us to suggest how the binding interactions of scaffolding and DNA with the coat shell may act to regulate the maturation process.

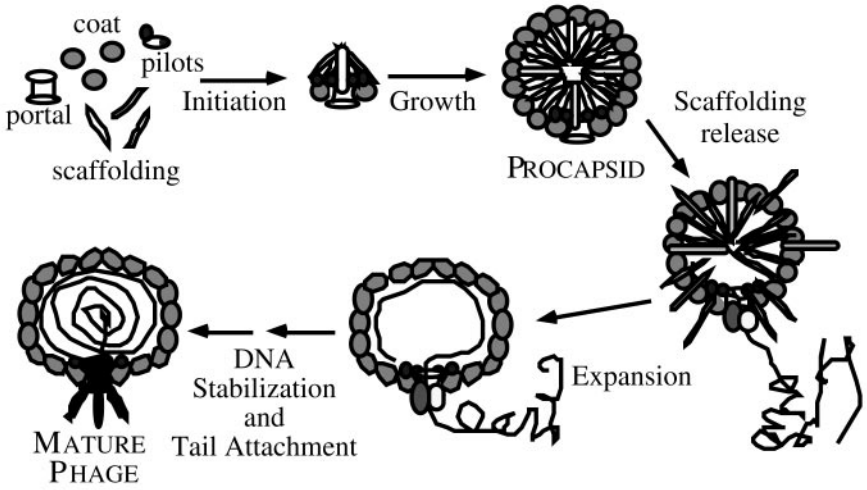

Figure 1. Schematic of the bacteriophage P22 assembly pathway.

Results

Three-dimensional reconstruction

Mutant scaffolding-containing procapsid and DNA-containing phage were prepared as described in Materials and Methods and imaged in a 400 kV electron cryomicroscope (Figure 2(a) and (b)). Suitable high-quality images of the procapsid and phage were processed, resulting in 15 Å procapsid and phage three-dimensional structures (Figure 3(a) and (b)). Both capsids form $T = 7$ icosahedral lattices composed of penton and hexon clusters. Overall, these structures are consistent with other P22 structures (Prasad *et al*., 1993; Thuman-Commike *et al*., 1996) except that, as described below, more detail is present due to the higher resolution of this study. Morphologically, as determined by Prasad *et al*. (1993), the procapsid has a thicker shell, and is both rounder and smaller than the thin-shelled polyhedral phage. Specifically, the procapsid has a maximal diameter of 610 Å, a minimal diameter of 588 Å, and an average diameter of 600 Å. However, the phage is polyhedral with a maximal diameter of 685 Å, a minimal diameter of 615 Å, and an average diameter of 650 Å corresponding to an average expansion of 10 %, consistent with previous results (Prasad *et al*., 1993). At this resolution, both the phage and procapsid have holes present in the center of the pentons and hexons. The holes in the phage, however, are approximately 15 Å in diameter compared to the 35-40 Å elongated procapsid holes. Thus, a closure of the procapsid hexon holes occurs during maturation but is not a complete closure as indicated by the previous 30 Å resolution structural studies of these capsids (Prasad *et al*., 1993).

Scaffolding-containing procapsid structure

The outer procapsid surface is covered with penton and skewed hexon clusters (Figure 4(a)). In the previous 19 Å procapsid structure (Thuman-Commike *et al*., 1996), the hexon contained a local 2-fold symmetry axis that did not intersect the center of the icosahedron. At this resolution, however, visual analysis shows that this local 2-fold symmetry is not as apparent. The subunits that form the hexon and penton clusters are composed of hairpin-like densities (Figure 4(a), green density). We cannot determine if a single hairpin or some other density division corresponds to one subunit of the coat protein gp5. However, to facilitate the description of these complex structures, we refer to the visually apparent hairpin-like density divisions and other visually apparent density shapes. Furthermore, we have color encoded these densities in the corresponding Figures using visually defined boundaries. Note, that neither the density naming nor coloring is intended to denote known subunit or domain boundaries for the P22 coat protein.

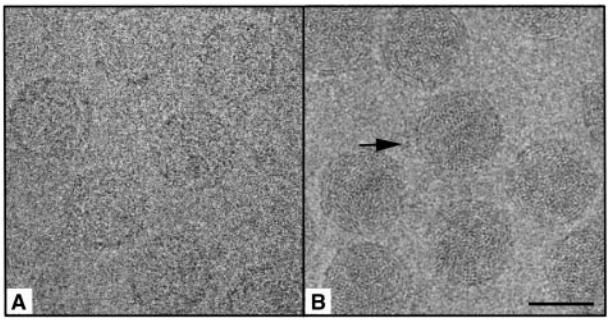

Figure 2. Electron cryomicroscopy image of bacteriophage P22 procapsid and phage. (a) The 400 kV images of the procapsid and (b) phage recorded at approximately 1.2 μm underfocus. The arrow indicates the tails at the 5-fold position. The scale bar represents 500 Å.

Of the six hexon hairpin-like densities, the two hairpins at opposite ends of the hexon long axis are closed (Figure 4(a), green density at one and seven o'clock positions), while the remaining four hairpins are open. At the base of each hairpin are two additional protruding densities. The first of these densities is a short, raised saddle-like region that connects pairs of hexon-hexon and hexon-penton hairpins from neighboring capsomeres (Figure 4(a), pink density). Each saddle is approximately 40 Å thick and connects hairpin pairs approximately 20 Å apart. The second density connected to the hairpin is a small ''knob-like'' density that extends into all strict and local 3-fold axes (Figure 4(a), orange density). Notice that these knobs also connect to adjacent hairpins within each hexon and penton.

On the inner surface of the procapsid, trimer clusters rather than hexon or penton clusters, dominate (Figure 4(b), purple density). These clusters connect neighboring hexon-hexon-hexon and hexon-penton-hexon trimers, linking three different capsomeres. Each of these clusters is located at the innermost radius within the procapsid, seeming to form inwardly protruding trimers within the procapsid, and depressed trimers on the procapsid outer surface. As described above, previous structural studies have located the wild-type scaffolding protein at the tips of four of these trimer clusters (Thuman-Commike *et al*., 1999a). The location of the scaffolding within this mutant scaffolding differs from the wild-type in that the scaffolding is located on all six hexon trimer cluster tips (Thuman-Commike *et al*., 2000). Although the scaffolding is not visible at the contour shown in Figure 4, modification of the contour threshold does allow visualization of the small finger-like densities protruding from the six hexon trimer cluster tips. Based on the localization of the scaffolding within this mutant scaffolding-containing procapsid, this density is attributed to the scaffolding protein (Thuman-Commike *et al*., 2000). In addition to the appearance of the trimer clusters, the inner surface has inwardly protruding finger-like densities surrounding each hexon hole (Figure 4(b), red density).

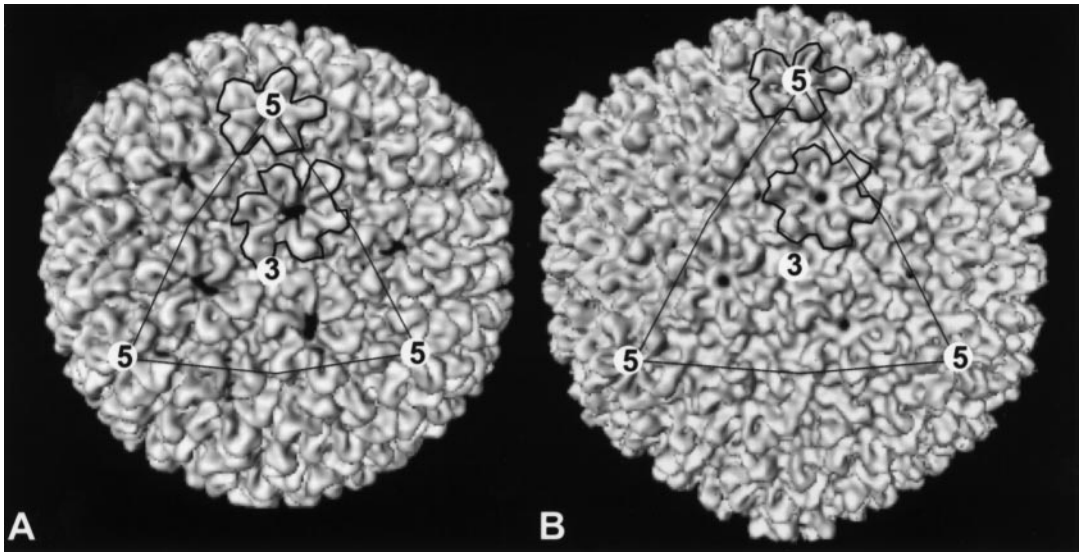

Figure 3. Surface representation of 15 Å resolution three-dimensional structures of the (a) procapsid and (b) phage with 5-fold and 3-fold axes marked. The thick outlines indicate the location of one penton and one hexon in each structure. The thin outlines denote the location of the unit triangle.

Phage structure

The outer phage surface is composed of hexon and penton clusters (Figure 4(c)). Unlike the procapsid, however, the hexons within the phage lattice are not skewed. That is, the hexons have undergone a symmetrization during maturation. In addition, the hexon hairpins that were closed in the procapsid have opened in the phage, and interact more closely with neighboring hairpins within each hexon and penton than with each other (Figure 4(c), green density). As with the procapsid, two additional densities protrude from each hairpin, forming saddles between hexon-hexon and hexon-penton subunits (Figure 4(c), pink density) and knobs at all strict and local 3-fold axes (Figure 4(c), orange density). In the phage, the saddles are more predominant than they were in the procapsid. Each saddle is approximately 20 Å thick, compared to 40 Å thick in the procapsid, and 45 Å long, compared to 20 Å long in the procapsid. The knobs present in the strict and local 3-fold axes are also more predominant in the phage because these densities no longer connect to neighboring hexon and penton hairpins and because the densities themselves are farther apart.

In contrast to the numerous features on the external surface, the inner phage surface exhibits no prominent features. One notable aspect is the density that surrounds each hexon hole. As mentioned above, the phage hexon hole is partially closed (Figure 4(c) and (d), red density), possibly as a result of an outward movement of the finger-like projections on the inner surface of the procapsid (Figure 4(b), red density).

DNA structure

Visual analysis of the phage images revealed that 5-fold views of the phage particles depict internal rings corresponding to the DNA (Figure 5(c)) that are not present in other views (Figure 5(a) and (b)). These rings are similar to DNA fingerprints observed in other DNA-containing phages, including bacteriophage T4 (Lepault *et al.*, 1987), bacteriophage T7 (Cerritelli *et al.*, 1997), and in both the herpesvirus capsid (Booy *et al.*, 1991) and virion (Zhou *et al.*, 1999).

Within our phage capsid shell there is a series of five full, and two disjoint, 10 Å thick, concentric shells (Figure 6). Given that rings are not present in all phage images, we decided to test if the observed shells were a result of the icosahedral averaging during three-dimensional reconstruction. To test this, we compared equivalent views of electron microscopy images to projection images computed from our phage reconstruction. This comparison (Figure 5) shows that the internal features of the electron cryomicroscopic images and the corresponding computed projection images are inconsistent. That is, with the exception of the 5-fold views (Figure 5(c), (f)), the projection images depict internal rings that the electron microscopy images do not. Consequently, as with similar results in herpesvirus (Zhou *et al.*, 1999), we consider the observed internal shell density a consequence of application of icosahedral symmetry to the internal DNA density within the phage capsid.

Maturation: comparison of procapsid and phage structures

The maturation transition from the procapsid to the phage results in several changes in both the conformations of individual coat protein subunits and the interactions between neighboring subunits (Figure 7). First, there is a decrease in the number of contacts within and between the hairpins forming the trimer clusters. Specifically, a decrease

occurs in the number of contacts in the connections of the small knob-like densities that extend from the base of each hairpin (Figure 7(a) and (b)). Second, there is a decrease in the procapsid shell thickness resulting in the thinner phage shell (Figure 7(c) and (d)). Third, the trimer clusters are raised outward and the shell thickness decreases. Fourth, the hexon and penton hairpins rotate, separate, and open (Figure 7(e) and (f), green densities). Last, the hexon hole diameter becomes smaller (Figure 7(e) and (f), red densities).

Discussion

DNA packing

A recent spool model for DNA packing within bacteriophage T7 proposes that the DNA is packed in a series of cylinders increasingly smaller in diameter parallel with the tail containing the 5-fold axis of the phage (Cerritelli *et al*., 1997). We observe five complete and two partial concentric shells within the phage structure (Figure 6). Our experimental results indicate this density is a result of the icosahedral averaging. Interestingly, however, the 25 Å spacing of these concentric shells is consistent with that observed in electron cryomicroscopy images and in solution X-ray scattering of phages (Earnshaw & Harrison, 1977; Thuman-Commike *et al*., 1999b). During our three-dimensional reconstruction process, the tail-containing 5-fold axis of each capsid is not aligned. Thus, if the DNA were arranged as cylinder-like densities, then during three-dimensional reconstruction, these cylinders would, in effect, be rotationally averaged together and result in the concentric shells we observe in our three-dimensional reconstruction. In contrast, other DNA packing models are not consistent with the observed ring-like patterns in our cryomicroscopy images, the observed concentric shells in our three-dimensional reconstruction, or with other experimental results. Specifically, in the liquid-crystal model (Lepault *et al*., 1987) one would expect the varying orientations of the crystalline domains to average out during the reconstruction, resulting in the appearance of disjoint density or noise within the capsid. In the case of the spiral-fold model (Black, 1989; Black *et al*., 1985), results from Raman spectroscopy of encapsidated P22 DNA (Aubrey *et al*., 1992) do not favor the sharp folds of this model. Furthermore, it is unlikely that such folded structures would appear as the concentric rings observed in our electron cryomicroscopic images. Consequently, we conclude that the appearance of concentric shells in our reconstruction is consistent with the spool model (Cerritelli *et al*., 1997; Harrison, 1983). Interestingly, previous electron microscopy and X-ray diffraction studies of bacteriophage T4 heads (Earnshaw *et al*., 1978) indicate that the DNA is also packaged as a spool, but with the spool axis perpendicular to, rather than parallel with the tail. In some of our phage images (Figure 2(b)), it is possible to identify the portal complex and tails when they are not oriented along the end-on view. Given that we observe concentric shells predominantly in images of particles with the icosahedral 5-fold view and without any visible portal complex and tails, we interpret our data to support the P22 DNA spool axis being parallel with the tail as for bacteriophage T7 (Cerritelli *et al*., 1997).

DNA packaging and maturation

These structures, in combination with previous results, suggest a mechanism by which the DNA is spooled into the capsid. We notice that the locations of the scaffolding viewed down a 5-fold axis from the inner procapsid surface appear as a series of rings (Figure 8). Each ring also consists of groups of four coat protein trimer tips, with an ~40 Å-wide groove between pairs of trimer clusters. We have previously proposed that the scaffolding resides as a tetramer over the top of this groove (Thuman-Commike *et al*., 1999a). Upon initiation of DNA packaging, DNA enters the procapsid at a 5-fold vertex that is the site of the DNA packaging portal (Bazinet & King, 1985). We propose that the DNA spools into the capsid by following the circular ring denoted by the coat groove and the scaffolding tetramers. Thus, both the inner coat network of grooves and the presence of the scaffolding act as a ''template'' for spooling the DNA around the inside surface of the coat protein shell. Visual examination of the inner coat network of grooves and the corresponding scaffolding identified many possible ''templates'' rather than a single predominant pathway. This organization of the DNA by the coat protein groove may be similar to the manner in which DNA is ordered by wrapping about the nucleosome core (Luger *et al*., 1997).

This mechanism implies that at least for P22, DNA packaging can only occur within the procapsid, and not the mature phage lattice, and requires the presence of the scaffolding protein. Consistent with this prediction, when DNA is lost *in vivo* from expanded capsids that lack one of the proteins required to plug the portal vertex, it is not repackaged (Strauss & King, 1984), and empty mature capsids cannot package DNA *in vitro* (Poteete *et al*., 1979). In addition, procapsids containing mutant scaffolding protein that leaks from the capsid prematurely, fail to package DNA (Greene & King, 1996). The presence of scaffolding may not be necessary for DNA packaging in all other dsDNA phages but, with the exception of T4 (Rao & Black, 1985), the need for an unexpanded procapsid appears to be a general requirement (Hohn & Hohn, 1974; Jardine *et al*., 1998; Masker & Serwer, 1982; Shibata *et al*., 1987). The fraction of the phage DNA packaged before the maturation transition occurs is roughly equivalent to the amount sufficient to coat the inner surface of the capsid with DNA in all cases (Bjornsti *et al*., 1983;

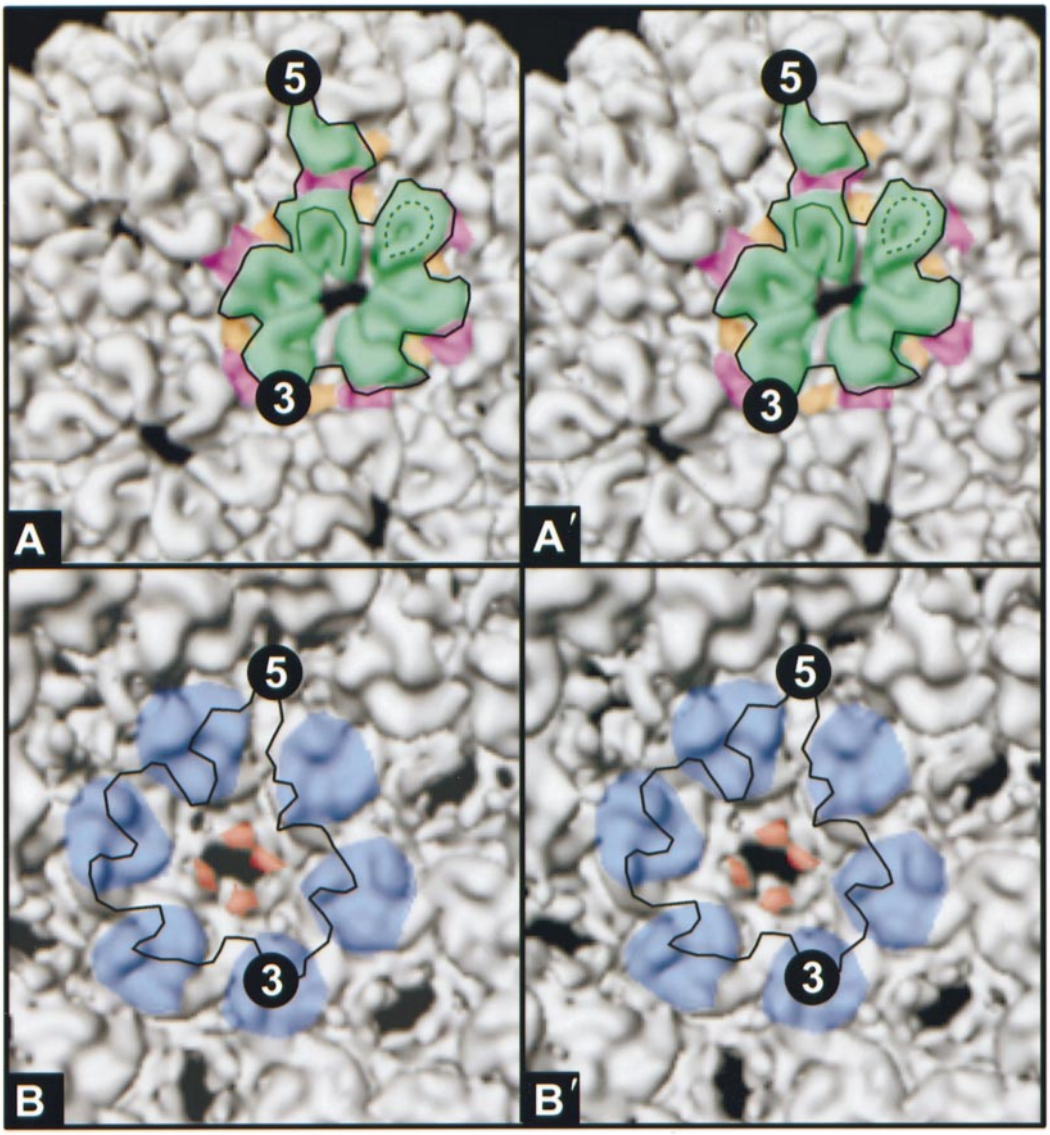

Figure 4 (*legend opposite*)

Earnshaw & Casjens, 1980; Hohn, 1983; Jardine & Coombs, 1998; Shibata *et al*., 1987). This is consistent with our model of packaging, as after the first layer of DNA enters the capsid, the presence of the template rings of the procapsid would no longer be required to package inner DNA layers.

How does the DNA insertion cause procapsid expansion? As the DNA contacts the scaffolding subunits, it may trigger their release through the hexon holes, most likely closing the holes by dragging the hexon fingers outward (Figure 7(g) and (h)). Since scaffolding/coat interactions appear to depend strongly upon interactions of charged residues (Parker & Prevelige, 1998), the close approach of the highly negatively charged DNA may trigger scaffolding release by counteracting these electrostatic interactions. This would then permit the transition to the expanded mature form, possessing a much smoother interior surface that would allow the DNA to be readily released upon infection of a host cell (King & Chiu, 1997).

Scaffolding/coat interactions and assembly

We propose that the most fundamental conformational change that occurs during expansion is the outward movement of the trimer clusters (Figure 7(c) and (d)) and that this movement can account for all the other maturation structural changes. Specifically, we observe that the raising of the trimer clusters at all strict and local 3-fold axes produces the flatter icosahedral faces and more polyhedral phage (Figure 3). The raised trimer clusters also increase the size of each icosahedral

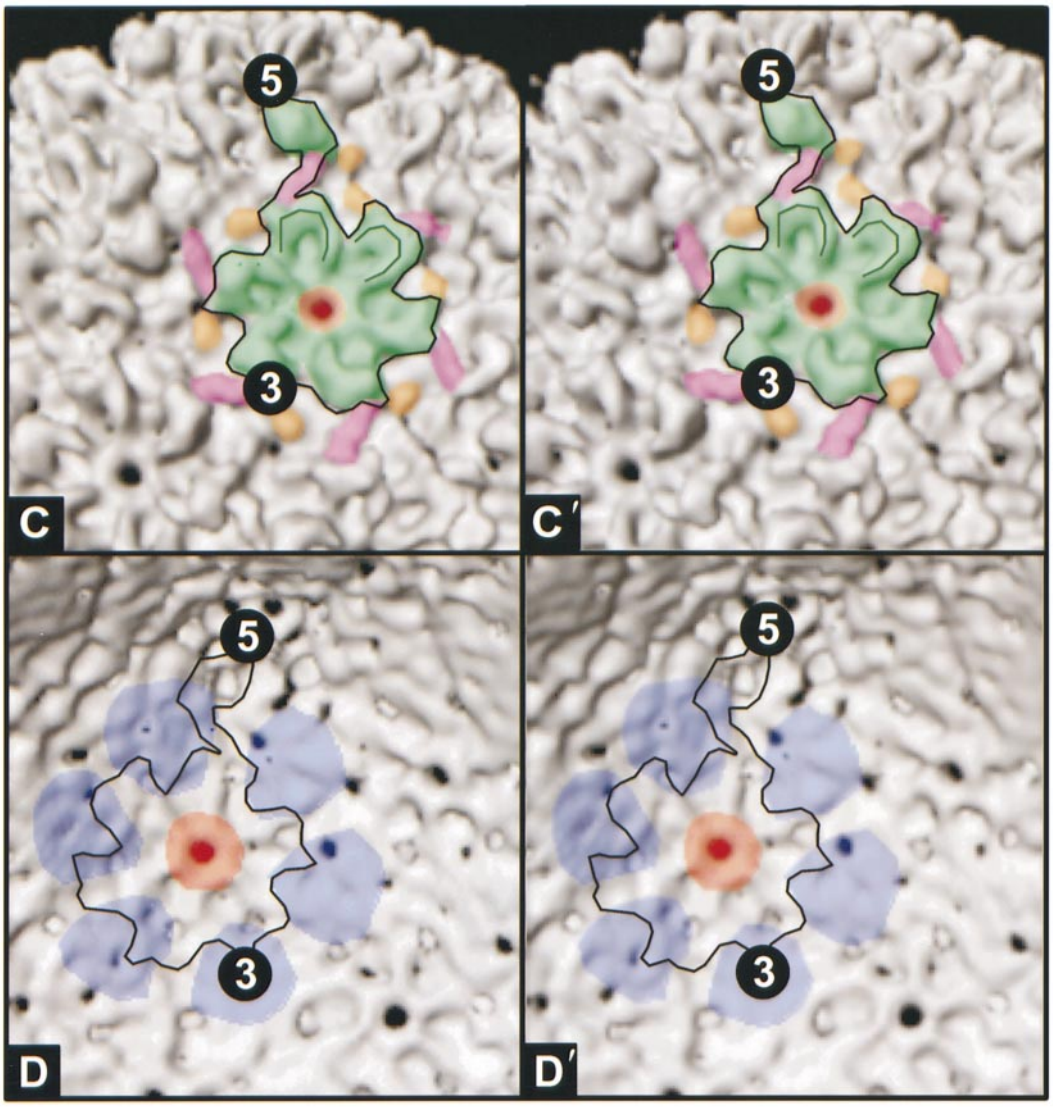

Figure 4. Stereo-pair views of the outer and inner surfaces of (a) and (b) procapsid, and (c) and (d) phage with the location of the 5-fold and 3-fold axes marked and the asymmetric unit outlined. The main structural features, which were identified through visual analysis of the three-dimensional map, are indicated in different colors. The coloring was performed based on visual inspection and is intended to facilitate the description of key structural components. It is not intended to indicate fixed domain boundaries or any subunit localizations within the capsids. On the outer surface, the green regions denote the upper hairpins of the penton and hexon subunits, the pink regions denote the saddles between hexon-hexon and hexon-penton subunits, the orange regions indicate the small arm of density extending from the base of each subunit in the strict and local 3-fold axes, and the red density denotes the visible portions of the internal density surrounding the hexon hole. On the inner surface, the procapsid trimer clusters are denoted in purple and the hexon finger-like densities are denoted in red. In addition, the dotted line marked on the green density in the outer surface procapsid view denotes the closed hairpins and the continuous lines marked on the green density in the outer surface of the procapsid and phage views denote the open hairpins.

face by enlarging the space between subunits at each strict and local 3-fold axes (Figure 4), producing the larger diameter phage. Last, the outward movement decreases the number of contacts within and between the subunits forming the trimer clusters, resulting in the rotation, separation and opening of the upper hexon hairpins. It is thus particularly intriguing that the trimer tips have also recently been identified as the binding sites for the scaffolding subunits (Thuman-Commike *et al.*, 1999a). Scaffolding release is required for capsid expansion and DNA packaging, as procapsids containing mutant scaffolding not released do not expand or package DNA *in vivo*, and are more difficult to expand *in vitro* (Greene & King, 1996). Proteolysis and removal of scaffolding also precedes expansion in phages T4 and λ (Black *et al.*, 1994; Zachary & Simon, 1977) as it would appear that binding of scaffolding at the trimer tips clamps the coat subunits into the procapsid conformation. This may serve to prevent the capsid from expanding until after the DNA enters and

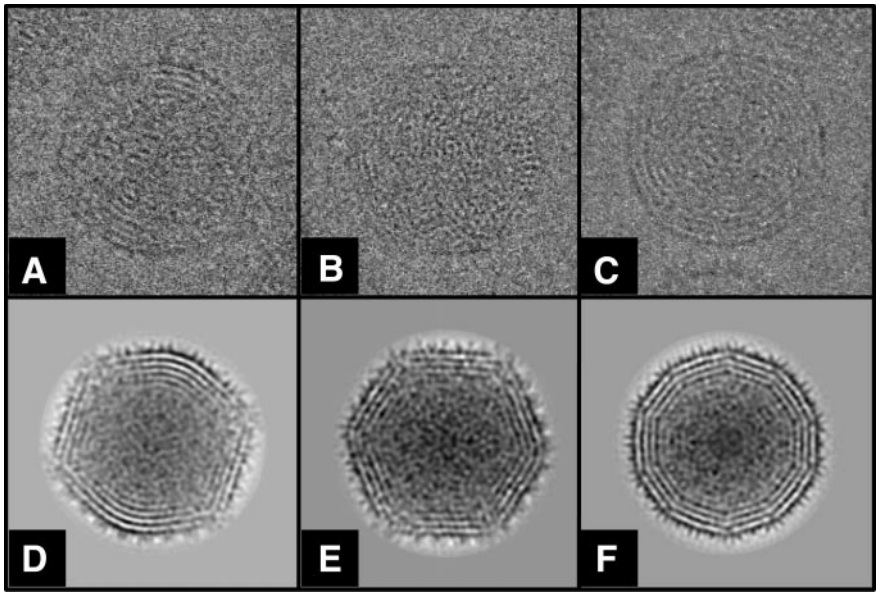

Figure 5. Comparison of individual phage particle images to computed projection images. (a)-(c) Individual electron cryomicroscopy particles images at 2, 3, and 5-fold views. (d)-(f) Corresponding views of computed projection images.

expels the scaffolding, ensuring that the capsid remains in a state competent for DNA packaging until then.

It is also significant that the coat subunits in the procapsid make more extensive contacts with each other at the trimer clusters, while in the phage, these interactions are diminished. Our previous model for procapsid assembly depends upon these trimer interactions, along with interactions between scaffolding subunits to regulate the assembly of a correctly sized procapsid (Thuman-Commike *et al*., 1999a). The trimer interactions may therefore be far more important at the procapsid stage than they are for the mature phage. In contrast, the interactions of coat subunits within capsomeres, *via* their hairpins, are more extensive in the phage than the procapsid, probably contributing to the greater stability of the phage. Interestingly, it is in the degree of opening of their hairpin-like densities that the seven coat subunit conformations are most obviously distinct in the procapsid. These distinctive hairpin conformations may be essential at the procapsid assembly stage to distinguish the seven quasi-equivalent coat conformations, and thus ensure formation of a correctly sized $T = 7$ procapsid. The more uniformly open hairpins of the phage coat subunits may make a more stable capsid, but are impossible to generate without error from soluble subunits. The presence of scaffolding during assembly presumably plays a significant role in generating the diverse hairpin conformations in coat subunits of the procapsid, since in the absence of scaffolding protein the coat subunits of both dsDNA phages and herpesvirus form aberrant structures or incorrectly sized capsids (Earnshaw & King, 1978; Matusick-Kumar *et al*., 1994; Ray & Murialdo, 1975; Roeder & Sadowski, 1977; Tatman *et al*., 1994; Thomsen *et al*., 1994).

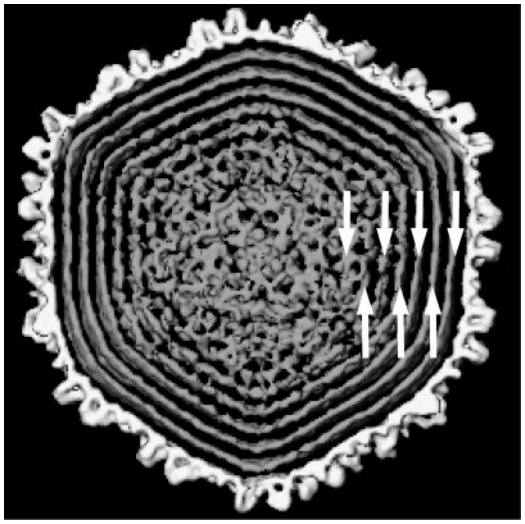

Figure 6. Central section of the phage three-dimensional reconstruction showing the observed concentric shells that correspond to the DNA. Five complete and two partial shells (arrows), each approximately 10 Å thick and approximately 25 Å apart, are present.

Similar mechanisms may regulate conformational transitions in other viruses. The binding of polioviruses to their receptors induces conformational changes that result in uncoating and RNA release (Chow *et al*., 1997). Interestingly, various single mutations in poliovirus coat proteins can lead to defects in both assembly and uncoating. One such mutant produces virions that are more labile to the

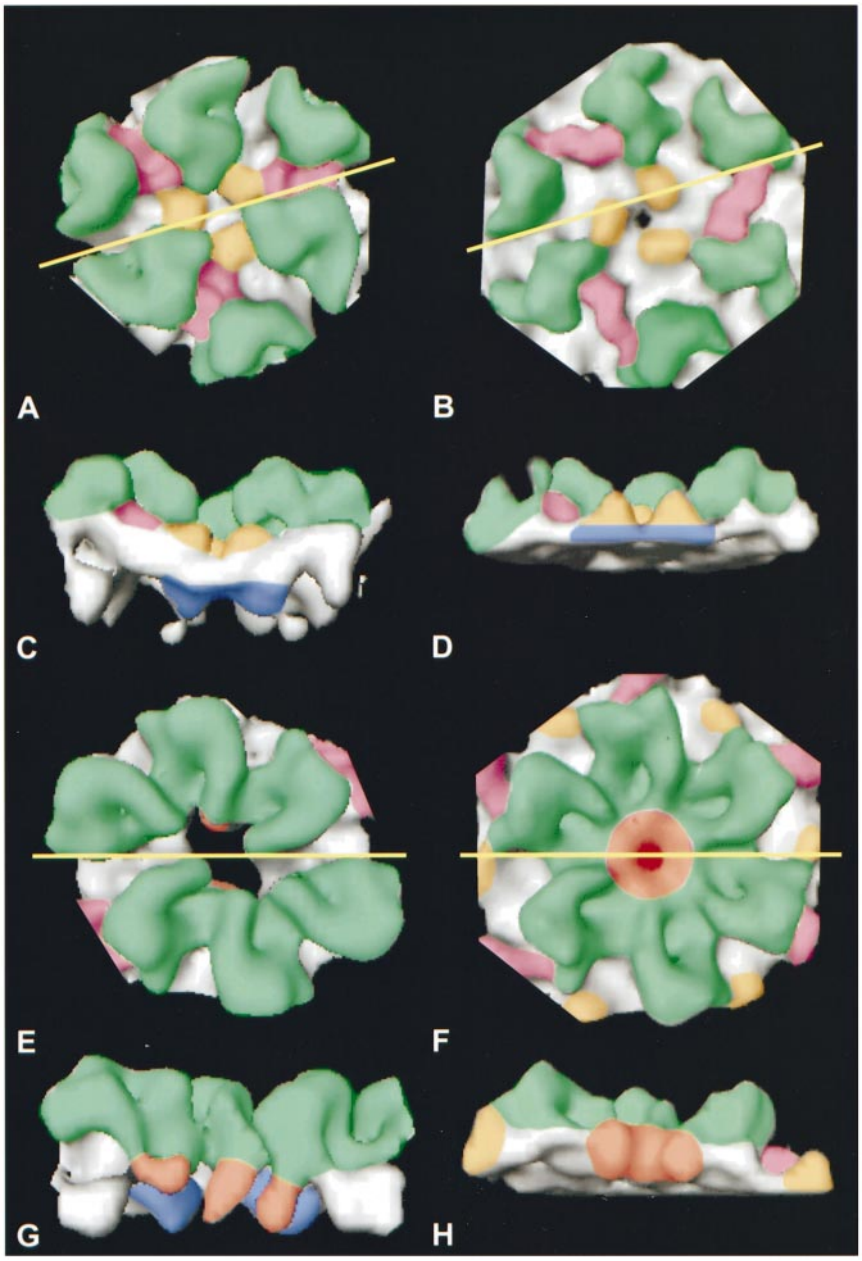

Figure 7. Computationally extracted views of the procapsid (left column) and phage (right column) structure. Each pair of rows depicts a selected region of the procapsid and phage viewed from the top (first row) and at 90° (second row) along the direction of the yellow line in the first row. In addition, the structures are color coded according to the key structural components outlined in the legend to Figure 4. The coloring was performed based on visual inspection and is intended to facilitate the description of key structural components. It is not intended to indicate fixed domain boundaries or any subunit localizations within the capsids. (a)-(d) Isolated trimer cluster interaction viewed down a 3-fold axis depicting the expansion that occurs at all strict and local 3-fold axes and the raising of the trimer clusters. (e)-(h) Isolated hexon depicting the regularization of the hexon and the closure of the hexon hole. Note that due to the curvature of the phage capsid, each hairpin within the hexon is viewed from a different angle. As a result, some of the hairpins may appear significantly different from others although they in fact are very similar.

uncoating transformation, and also results in accumulation of many pentameric assembly intermediates that cannot proceed to form virions (Moscufo & Chow, 1992). The non-assembly competent dimers and trimers produced by several temperature-sensitive P22 coat proteins may represent the same class of defect (Teschke & King, 1995). Conformational changes in poliovirus can also be regulated by the binding of external factors, such as antiviral drugs that can block the uncoating step and stabilize the virus against transition *in vitro* (Grant *et al.*, 1994). The binding site for these compounds is normally occupied by small lipid molecules called pocket factors that stabilize

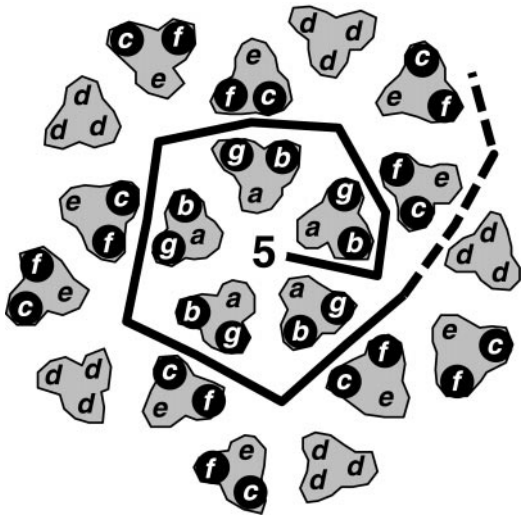

Figure 8. Schematic of the procapsid icosahedral lattice viewed from the internal 5-fold axis. The outlines indicate the positions of the internal trimer clusters with labels denoting each of the seven quasi-equivalent coat protein subunits. Scaffolding-bound subunits are denoted with black circles and the proposed DNA path in our DNA packaging/expansion model is shown by the thick line.

the virus (Mosser & Rueckert, 1993). Scaffolding proteins could be considered as a form of pocket factor.

These new improved-resolution structures of P22 procapsids and phage therefore provide information on the structural mechanism of the maturation transition, as well as reveal a rationale for such a transition to exist. Although the phage structure provides the increased stability required for protection of the DNA, it lacks the structural features needed to distinguish the coat subunit conformations for correct assembly, and to provide a template surface for DNA packaging. The procapsid may be a metastable intermediate, but it also appears optimally designed for efficient assembly and operation as a DNA packaging machine.

Materials and Methods

Sample preparation

P22 procapsids were prepared as described by Thuman-Commike *et al*. (1999b) from a phage strain carrying a temperature-sensitive mutation in the scaffolding protein gene, L177I, which impairs scaffolding release from the procapsid. Mature P22 phage were prepared as described by Thuman-Commike *et al*. (1999b).

Electron cryomicroscopy and image processing

Purified capsids were prepared for electron cryomicroscopy using standard procedures (Adrian *et al*., 1984; Dubochet *et al*., 1988). In the case of the phage, holey carbon grids coated with a thin layer of evaporated carbon were used. Samples were imaged on a JEOL 4000 with 400 kV electrons at −168 °C. Procapsids were imaged at 50,000× and the phage at 40,000× using flood-beam imaging. Images were recorded on Kodak SO-163 film, developed in full-strength Kodak developer D19 for 12 minutes at 20 °C, and fixed for ten minutes in Kodak fixer.

Images were scanned on a Zeiss SCAI microdensitometer (Carl Zeiss, Inc., Englewood, CO) with a step size of 14 μm, corresponding to scan sizes of 2.8 Å/pixel for the procapsid, and 3.5 Å/pixel for the phage. For each suitable micrograph, defocus was assessed by locating the contrast transfer function rings in the average power spectrum (Zhou *et al*., 1996). For the procapsid, 11 micrographs with defocus values ranging from 0.9-1.4 μm were used and for the phage, 15 micrographs with defocus values ranging from 0.9-1.3 μm underfocus were used. Images were processed as described (Crowther *et al*., 1970; Fuller, 1987; Thuman-Commike & Chiu, 1997; Thuman-Commike *et al*., 1996) resulting in the determination of 697 procapsid orientations and 720 phage orientations. Full icosahedral symmetry was imposed in real space after three-dimensional reconstruction (Fuller, 1987). Adequate Fourier space sampling was ensured by analyzing the inverse eigenvalue spectrum calculated during the interpolation step of the Fourier Bessel analysis of the final reconstructions (Crowther, 1971). The final resolution was assessed as the point at which the amplitude-weighted mean phase difference between two independent reconstructions reached 45° (Baker *et al*., 1990; Frank *et al*., 1981).

Acknowledgments

This work was supported by the Institute of Allergy and Infectious Disease of the National Institutes of Health (AI43656 to W.C.), the National Center for Research Resources of the National Institutes of Health (P41RR02250 to W.C.), and the Institute of General Medical Science of the National Institutes of Health (GM17980 to J.K and GM47980 to P.E.P).

References

Adrian, M., Dubochet, J., Lepault, J. & McDowall, A. W. (1984). Cryo-electron microscopy of viruses. *Nature,* **308**, 32-36.

Aubrey, K. L., Casjens, S. R. & Thomas, G. J., Jr (1992). Secondary structure and interactions of the packaged dsDNA genome of bacteriophage P22 investigated by Raman difference spectroscopy. *Biochemistry*, **31**, 11835-11842.

Baker, T. S., Newcomb, W. W., Booy, F. P., Brown, J. C. & Steven, A. C. (1990). Three-dimensional structures of maturable and abortive capsids of equine herpesvirus 1 from cryoelectron microscopy. *J. Virol.* **64**, 563-573.

Bazinet, C. & King, J. (1985). The DNA translocating vertex of dsDNA bacteriophage. *Annu. Rev. Microbiol.* **39**, 109-129.

Bjornsti, M.-A., Reilly, B. E. & Anderson, D. L. (1983). Morphogenesis of bacteriophage ϕ29 of *Bacillus subtilus*: oriented and quantized *in vitro* packaging of DNA protein gp3. *J. Virol.* **45**, 383-396.

Black, L. W. (1989). DNA packaging in dsDNA bacteriophages. *Annu. Rev. Microbiol.* **43**, 267-292.

Black, L. W., Newcomb, W. W., Boring, J. W. & Brown, J. C. (1985). Ion etching of bacteriophage T4: support for a spiral-fold model of packaged DNA. *Proc. Natl Acad. Sci. USA,* **82**, 7960-7964.

Black, L. W., Showe, M. K. & Steven, A. C. (1994). Morphogenesis of the T4 head. In *Molecular Biology of Bacteriophage T4* (Karam, J. D., ed.), 2nd edit., pp. 218-258, ASM Press, Washington, DC.

Booy, F. P., Newcomb, W. W., Trus, B. L., Brown, J. C., Baker, T. S. & Steven, A. C. (1991). Liquid-crystalline, phage-like packing of encapsidated DNA in herpes simplex virus. *Cell,* **64**, 1007-1015.

Casjens, S. & Hendrix, R. (1988). Control mechanisms in dsDNA bacteriophage assembly. In *The Bacteriophages* (Calender, R., ed.), vol. 1, pp. 15-91, Plenum Publishing, New York.

Casjens, S. & King, J. (1974). P22 morphogenesis. I: catalytic scaffolding protein in capsid assembly. *J. Supramol. Struct.* **2**, 202-224.

Cerritelli, M. E., Cheng, N., Rosenberg, A. H., McPherson, C. E., Booy, F. P. & Steven, A. C. (1997). Encapsidated conformation of bacteriopahge T7 DNA. *Cell,* **91**, 271-280.

Chow, M., Basavappa, R. & Hogle, J. M. (1997). The role of conformational transitions in poliovirus pathogenesis. In *Structural Biology of Viruses* (Chiu, W., Burnett, R. M. & Garcea, R. L., eds), pp. 157-186, Oxford University Press, New York.

Conway, J. F., Duda, R. L., Hendrix, R. W. & Steven, A. C. (1995). Proteolytic and conformational control of virus capsid maturation: the bacteriophage HK97 system. *J. Mol. Biol.* **253**, 86-99.

Crowther, R. A. (1971). Procedures for three-dimensional reconstruction of spherical viruses by Fourier synthesis from electron micrographs. *Phil. Trans. Roy. Soc. ser. B.* **261**, 221-230.

Crowther, R. A., DeRosier, D. J. & Klug, A. (1970). The reconstruction of a three-dimensional structure from projections and its application to electron microscopy. *Proc. Roy. Soc. London,* **317**, 319-340.

D'Halluin, J.-C. M., Martin, G. R., Torpier, G. & Boulanger, P. (1978). Adenovirus type 2 assembly analysed by reversible cross-linking of labile intermediates. *J. Virol.* **26**, 357-363.

DiIanni, C. L., Drier, D. A., Deckman, I. C., McCann, P. J., Liu, F., Roizman, B., Colonno, R. J. & Cordingley, M. G. (1993). Identification of the herpes simplex virus-1 protease cleavage sites by direct sequence analysis of autoproteolytic cleavage products. *J. Biol. Chem.* **268**, 2048-2051.

Dokland, T. & Murialdo, H. (1993). Structural transitions during maturation of bacteriophage lambda capsids. *J. Mol. Biol.* **233**, 682-694.

Dubochet, J., Adrian, M., Chang, J. J., Homo, J. C., Lepault, J., McDowall, A. W. & Schultz, P. (1988). Cryo-electron microscopy of vitrified specimens. *Quart. Rev. Biophys.* **21**, 129-228.

Earnshaw, W. & Casjens, S. (1980). DNA packaging by double stranded DNA bacteriophages. *Cell,* **21**, 319-325.

Earnshaw, W. & Harrison, S. C. (1977). DNA arrangement in isometric phage heads. *Nature,* **268**, 598-602.

Earnshaw, W. & King, J. (1978). Structure of phage P22 coat protein aggregates formed in the absence of the scaffolding protein. *J. Mol. Biol.* **126**, 721-747.

Earnshaw, W., King, J., Harrison, S. C. & Eiserling, F. A. (1978). The structural organization of DNA packed within the heads of T4 wild type, isometric, and giant bacteriophages. *Cell,* **14**, 559-568.

Frank, J., Verschoor, A. & Boublik, M. (1981). Computer averaging of electron micrographs of 40*S* ribosomal subunits. *Science,* **214**, 1353-1355.

Fuller, S. D. (1987). The $T = 4$ envelope of Sindbis virus is organized by interactions with a complementary $T = 3$ capsid. *Cell,* **48**, 923-934.

Galisteo, M. L. & King, J. (1993). Conformational transformations in the protein lattice of phage P22 procapsids. *Biophys. J.* **65**, 227-235.

Grant, R. A., Hiremath, C. N., Filman, D. J., Syed, R., Andries, K. & Hogle, J. M. (1994). Structures of poliovirus complexes with antiviral drugs: implications for viral stability and drug design. *Curr. Biol.* **4**, 784-797.

Greene, B. & King, J. (1996). Scaffolding mutants identifying domains required for P22 procapsid assembly and maturation. *Virology,* **225**, 82-96.

Harrison, S. C. (1983). Packaging of DNA into bacteriophage heads: a model. *J. Mol. Biol.* **171**, 577-580.

Hohn, B. (1983). DNA sequences necessary for packaging of bacteriophage l DNA. *Proc. Natl Acad. Sci. USA,* **80**, 7456-7460.

Hohn, B. & Hohn, T. (1974). Activity of empty, headlike particles for packaging of DNA of bacteriophage. *Proc. Natl Acad. Sci. USA,* **71**, 2372-2376.

Incardona, N. L. & Kaesberg, P. (1964). A pH-induced structural change in bromegrass mosaic virus. *Biophys. J.* **4**, 11-21.

Jardine, P. J. & Coombs, D. H. (1998). Capsid expansion follows the initiation of DNA packaging in bacteriophage T4. *J. Mol. Biol.* **284**, 661-672.

Jardine, P. J., McCormick, M. C., Lutze-Wallace, C. & Coombs, D. H. (1998). The bacteriophage T4 DNA packaging apparatus targets the unexpanded prohead. *J. Mol. Biol.* **284**, 647-659.

King, J. & Casjens, S. (1974). Catalytic head assembling protein in virus morphogenesis. *Nature,* **251**, 112-119.

King, J. & Chiu, W. (1997). The procapsid transition in double-stranded DNA bacteriophages. In *Structural Biology of Viruses* (Chiu, W., Burnett, R. M. & Garcea, R. L., eds), pp. 288-311, Oxford University Press, New York.

Lepault, J., Dubochet, J., Baschong, W. & Kellenberger, E. (1987). Organization of double-stranded DNA in bacteriophages: a study by cryo-electron microscopy of vitrified samples. *EMBO J.* **6**, 1507-1512.

Luger, K., Mader, A. W., Richmond, R. K., Sargent, D. F. & Richmond, T. J. (1997). Crystal structure of the nucleosome core particle at 2.8 Å resolution. *Nature,* **389**, 251-260.

Masker, W. E. & Serwer, P. (1982). DNA packaging *in vitro* by an isolated bacteriophage T7 procapsid. *J. Virol.* **43**, 1138-1142.

Matusick-Kumar, L., Hurlburt, W., Weinheimer, S. P., Newcomb, W. W., Brown, J. C. & Gao, M. (1994). Phenotype of the herpes simplex virus type-1 protease substrate ICP35 mutant virus. *J. Virol.* **68**, 5384-5394.

Moscufo, N. & Chow, M. (1992). Myristate-protein interactions in poliovirus: interactions of VP4 threonine-28 contribute to the structural conformation of assembly intermediates and the stability of assembled virions. *J. Virol.* **66**, 6849-6857.

Mosser, A. G. & Rueckert, R. R. (1993). WIN 51711-dependent mutants of poliovirus type 3: evidence

that virions decay after release from cells unless drug is present. *J. Virol.* **67**, 1246-1254.

Nelson, R. A., Reilly, B. E. & Anderson, D. L. (1976). Morphogenesis of bacteriophage ϕ29 of *Bacillus subtilis*: preliminary isolation and characterization of intermediate particles of the assembly pathway. *Virology,* **19**, 518-532.

Onorato, L. & Showe, M. K. (1975). Gene *gp*21 protein-dependent proteolysis *in vitro* of purified gene *gp*22 product of bacteriophage T4. *J. Mol. Biol.* **92**, 395-412.

Parker, M. H. & Prevelige, P. E., Jr (1998). Electrostatic interactions drive scaffolding/coat binding and procapsid maturation in bacteriophage P22. *Virology,* **250**, 337-349.

Poteete, A. R., Jarvik, V. & Botstein, D. (1979). Encapsulation of phage P22 DNA *in vitro*. *Virology,* **95**, 550-564.

Prasad, B. V. V., Prevelige, P. E., Marietta, E., Chen, R. O., Thomas, D., King, J. & Chiu, W. (1993). Three-dimensional transformation of capsids associated with genome packaging in a bacterial virus. *J. Mol. Biol.* **231**, 65-74.

Ray, P. & Murialdo, H. (1975). The role of gene Nu3 in bacteriophage lambda head morphogenesis. *Virology,* **64**, 247-263.

Rao, V. B. & Black, L. W. (1985). DNA packaging of bacteriophage T4 proheads in vitro. Evidence that prohead expansion is not coupled to DNA packaging. Calorimetric comparison of successive conformational states of the gp23 surface lattice of bacteriophage T7. *J. Mol. Biol.* **185**, 565-578.

Rixon, F. J. (1993). Structure and assembly of herpesviruses. *Sem. Virol.* **4**, 135-144.

Robinson, I. K. & Harrison, S. C. (1982). Structure of the expanded state of tomato bushy stunt virus. *Nature,* **297**, 563-568.

Roeder, G. S. & Sadowski, P. D. (1977). Bacteriophage T7 morphogenesis: Phage-related particles in cells infected with wild-type and mutant T7 phage. *Virology,* **76**, 263-285.

Ross, P. D., Black, L. W., Bisher, M. E. & Steven, A. C. (1985). Assembly-dependent conformational changes in a viral capsid protein. *J. Mol. Biol.* **183**, 353-364.

Rueckert, R. R. (1996). Picornaviridae: the viruses and their replication. In *Virology* (Fields, B. N. & Knipe, D. N., eds), 3rd edit., pp. 609-654, Lippincott-Raven, New York.

Shibata, H., Fujisawa, H. & Minagawa, T. (1987). Characterization of the bacteriophage T3 DNA packaging reaction *in vitro* in a defined system. *J. Mol. Biol.* **196**, 845-851.

Steven, A. C., Greenstone, H. L., Booy, F. P., Black, L. W. & Ross, P. D. (1992). Conformational changes of a viral capsid protein. Thermodynamic rationale for proteolytic regulation of bacteriophage T4 capsid expansion, co-operativity, and super-stabilization by soc binding. *J. Mol. Biol.* **228**, 870-884.

Strauss, H. & King, J. (1984). Steps in the stabilization of newly packaged DNA during phage P22 morphogenesis. *J. Mol. Biol.* **172**, 523-543.

Tatman, J. D., Preston, V. G., Nicholson, P., Elliott, R. M. & Rixon, F. J. (1994). Assembly of herpes simplex virus type 1 capsids using a panel of recombinant baculoviruses. *J. Gen. Virol.* **75**, 1101-1113.

Teschke, C. M. & King, J. (1995). *In vitro* folding of phage P22 coat protein with amino acid substitutions that confer *in vivo* temperature sensitivity. *Biochemistry,* **34**, 6815-6826.

Thomsen, D. R., Roof, L. L. & Homa, F. L. (1994). Assembly of herpes simplex virus (HSV) intermediate capsids in insect cells infected with recombinant baculoviruses expressing HSV capsid proteins. *J. Virol.* **68**, 2442-2457.

Thuman-Commike, P., Greene, B., Malinski, J., Burbea, M., McGough, A., Chiu, W. & Prevelige, P. E., Jr (1999a). Mechanism of scaffolding-directed virus assembly suggested by comparison of scaffolding-containing and scaffolding-lacking P22 procapsids. *Biophys. J.* **76**, 3267-3277.

Thuman-Commike, P. A. & Chiu, W. (1997). Improved common line-based icosahedral virus particle image orientation estimation algorithms. *Ultramicroscopy,* **68**, 231-255.

Thuman-Commike, P. A., Greene, B., Jakana, J., Prasad, B. V., King, J., Prevelige, P. E., Jr & Chiu, W. (1996). Three-dimensional structure of scaffolding-containing phage P22 procapsids by electron cryomicroscopy. *J. Mol. Biol.* **260**, 85-98.

Thuman-Commike, P. A., Tsuruta, H., Greene, B., Prevelige, P. E., Jr, King, J. & Chiu, W. (1999b). Solution X-ray scattering-based estimation of electron cryomicroscopy imaging parameters for three-dimensional reconstruction. *Biophys. J.* **76**, 2249-2261.

Thuman-Commike, P. A., Greene, B., Jakana, J., McGough, A., Prevelige, P. E. & Chiu, W. (2000). Identification of additional coat/scaffolding interactions in a bacteriophage p22 mutant defective in maturation. *J Virol.* In the press.

Trus, B. L., Booy, F. P., Newcomb, W. W., Brown, J. C., Homa, F. L., Thomsen, D. R. & Steven, A. C. (1996). The herpes simplex virus procapsid: structure, conformational changes upon maturation, and roles of the triplex proteins V19c and VP23 in assembly. *J. Mol. Biol.* **263**, 447-462.

Tuma, R., Prevelige, P. E, Jr & Thomas, G. J. J. (1998). Mechanism of capsid maturation in a double-stranded DNA virus. *Proc. Natl Acad. Sci. USA,* **95**, 9885-9890.

Zachary, A. & Simon, L. (1977). Size changes among lambda capsid precursors. *Virology,* **81**, 107-116.

Zhou, Z. H., Chen, D. H., Jakana, J., Rixon, F. J. & Chiu, W. (1999). Visualization of tegument-capsid interactions and DNA in intact herpes simplex virus type 1 virions. *J. Virol.* **73**, 3210-3218.

Zhou, Z. H., Hardt, S., Wang, B., Sherman, M. B., Jakana, J. & Chiu, W. (1996). CTF determination of images of ice-embedded single particles using a graphics interface. *J. Strs. Biol.* **116**, 216-222.

Edited by W. Baumeister

(Received 5 August 1999; received in revised form 31 January 2000; accepted 7 February 2000)